Modal Processor Effects Inspired by Hammond Tonewheel Organs

Werner, K. J., & Abel, J. S. (2016). Modal Processor Effects Inspired by Hammond Tonewheel Organs. *Applied Sciences*, *6*(7), [185]. https://doi.org/10.3390/app6070185

Published in:
Applied Sciences

Document Version:
Publisher's PDF, also known as Version of record

applied sciences

MDPI

Article

Modal Processor Effects Inspired by Hammond Tonewheel Organs

Kurt James Werner * and Jonathan S. Abel

Center for Computer Research in Music and Acoustics (CCRMA), Department of Music, Stanford University, 660 Lomita Drive, Stanford, CA 94305-8180, USA; abel@ccrma.stanford.edu

* Correspondence: kwerner@ccrma.stanford.edu; Tel.: +1-650-723-4971

Academic Editor: Vesa Valimaki

Received: 16 March 2016; Accepted: 13 June 2016; Published: 28 June 2016

Abstract: In this design study, we introduce a novel class of digital audio effects that extend the recently introduced modal processor approach to artificial reverberation and effects processing. These pitch and distortion processing effects mimic the design and sonics of a classic additive-synthesis-based electromechanical musical instrument, the Hammond tonewheel organ. As a reverb effect, the modal processor simulates a room response as the sum of resonant filter responses. This architecture provides precise, interactive control over the frequency, damping, and complex amplitude of each mode. Into this framework, we introduce two types of processing effects: pitch effects inspired by the Hammond organ's equal tempered "tonewheels", "drawbar" tone controls, vibrato/chorus circuit, and distortion effects inspired by the pseudo-sinusoidal shape of its tonewheels and electromagnetic pickup distortion. The result is an effects processor that imprints the Hammond organ's sonics onto any audio input.

Keywords: audio signal processing; modal analysis; room acoustics; signal analysis; artificial reverberation; digital audio effects; virtual analog; musical instruments

1. Introduction

The Hammond tonewheel organ is a classic electromechanical musical instrument, patented by Laurens Hammond in 1934 [1]. Although it was intended as an affordable substitute for church organs [2], it has also become widely known as an essential part of jazz (where it was popularized by Jimmy Smith), R & B and rock music (where the Hammond playing of Keith Emerson of Emerson, Lake & and Palmer and Jon Lord of Deep Purple is exemplary). The most popular model is the Hammond B-3, although many other models exist [3]. The sound of the Hammond organ is rich and unusual. Its complexity comes from the Hammond organ's unique approach to timbre and certain quirks of its construction.

In this article, we describe a novel class of modal-processor-based audio effects which we call the "Hammondizer". The Hammondizer can imprint the sonics of the Hammond organ onto any sound; it mimics and draws inspiration from the architecture of the Hammond tonewheel organ. We begin by describing the architecture and sonics of the Hammond tonewheel organ alongside related work on Hammond organ modeling.

The Hammond organ is essentially an additive synthesizer. Additive synthesizers create complex musical tones by adding together sinusoidal signals of different frequencies, amplitudes, and phases [4]. In the Hammond organ, 91 sinusoidal signals are available. These sinusoids are created when "tonewheels"—ferromagnetic metal discs—spin and the pattern of ridges cut into their edges is transduced by electromagnetic pickups into electrical signals, a technique originated in Thaddeus Cahill's late-19th century instrument, the Telharmonium [5]. Hammond organ tonewheel pickups have not been studied much in particular, but modeling and simulation of electromagnetic pickups in

general is an active research area [6–10]. Any nonlinearities in a pickup model will cause bandwidth expansion and add to the characteristic sound of the Hammond organ. In the case that this bandwidth expansion would go beyond the Nyquist limit, alias-suppression methods become relevant [11–14].

These 91 tonewheels are tuned approximately to the twelve-tone equal-tempered musical scale [15]—In scientific pitch notation, the lowest-frequency tonewheel on a Hammond organ is tuned to C1 (≈32.7 Hz) and the highest-frequency tonewheel is tuned to F#7 (≈5919.9 Hz) [16]. The lowest octave of tonewheels do not form sinusoids, but more complex tones that have strong 3rd and 5th harmonics, making them closer to square waves than sine waves [15]. Some aficionados have pointed to crosstalk between nearby tonewheel/pickup pairs as an important sonic feature of the Hammond organ [17,18].

The tone of the Hammond organ is set using nine "drawbars". Unlike traditional organs, where "stops" bring in entire complex organ sounds, the Hammond organ's drawbars set the relative amplitudes of individual sinusoids in a particular timbre. These nine sinusoids form a pseudo-harmonic series summarized in Table 1 [19]. This pseudo-harmonic series deviates from the standard harmonic series in three ways: (1) each overtone is tuned to the nearest available tonewheel; (2) certain overtones are omitted, especially the 6th harmonic, which would be between the 8th and 9th drawbar); and (3) new fictitious overtones are added (the 5th and sub-octave).

Table 1. Hammond Organ Drawbars—Pitch in organ stop lengths and musical intervals.

Pipe Pitch	**16′**	**5⅓′**	**8′**	**4′**	**2⅔′**	**2′**	**1⅗′**	**1⅓′**	**1′**
Scale Interval	sub-octave	5th	Unison	8th	12th	15th	17th	19th	22nd
Stop Name	Bourdon	Quint	Principal	Octave	Nazard	Block Flöte	Tierce	Larigot	Sifflöte
Semitone Offset	−12	+7	0	+12	+19	+24	+28	+31	+36
Error E (cents)	N/A	N/A	0	0	−1.955	0	+13.686	−1.955	0

The raw sound of the Hammond organ tonewheels is static. To enrich the sound, Hammond added a chorus/vibrato circuit [20]. Earlier models used a tremolo effect in place of the chorus/vibrato circuit [21]. The sound was further enriched by an electro-mechanical spring reverb device [22]. Although Hammond did not originally approve of the practice, it became customary to play Hammond organs through a Leslie speaker, an assembly with a spinning horn and baffle that creates acoustic chorus and tremolo effects. The Leslie speaker has been covered extensively in the modeling literature. Various approaches have involved interpolating delay lines [23,24] and amplitude modulation [25,26], perception-based models [28], and time-varying Finite Impulse Response (FIR) filters [29]. Recently, Pekonen et al. presented a novel Leslie model [18] using spectral delay filters [30]. Werner et al. used the Wave Digital Filter approach to model the Hammond vibrato/chorus circuit [31].

Although Hammond had stopped manufacturing their tonewheel organs by 1975, the Hammond sound remained influential. Many manufacturers developed clones of the Hammond tonewheel organ [17,32–35]. Commercial efforts have been accompanied by popular and academic work in virtual analog modeling [36]. Gordon Reid wrote a series of articles for *Sound on Sound* on generic synthesis approaches to modeling aspects of the Hammond organ [17,32–35]. Pekonen et al. studied efficient methods for digital tonewheel organ synthesis [18].

The Hammondizer audio effect is implemented as an extension to the recently-introduced "modal reverberator" approach to artificial reverberation [37–40]. Although there are many other approaches to modal sound synthesis in the literature (e.g., [41–44], the choice to extend the modal reverberator architecture to create the Hammondizer effect was a natural one for two reasons: (1) there are strong similarities between the system architecture of the Hammond organ and the system architecture of the modal reverberator; (2) the modal reverberator is already formulated as an audio effect which processes rather than synthesizes sound.

The rest of the article is structured as follows. Section 2 presents a simplified system architecture of the Hammond organ, Section 3 reviews relevant aspects of the modal processor approach,

Section 4 presents the novel Hammondizer digital audio effect, Section 5 demonstrates features of the Hammondizer through a series of examples, and Section 6 concludes.

2. Hammond Organ System Architecture

Here we extend the qualitative description above and present a mathematical formulation of the basic operation of the Hammond tonewheel organ. Referring to Figure 1, the player controls the organ by depressing keys on a standard musical keyboard shown on the left. Each of its 61 keys has a note on/off state $n_k(t) \in [0, 1]$ that is indexed by a key number $k \in [1 \cdots 61]^\top$; these are collected into a column $\boldsymbol{n}(t)$. Here and in the rest of the article, t is the discrete time sample index.

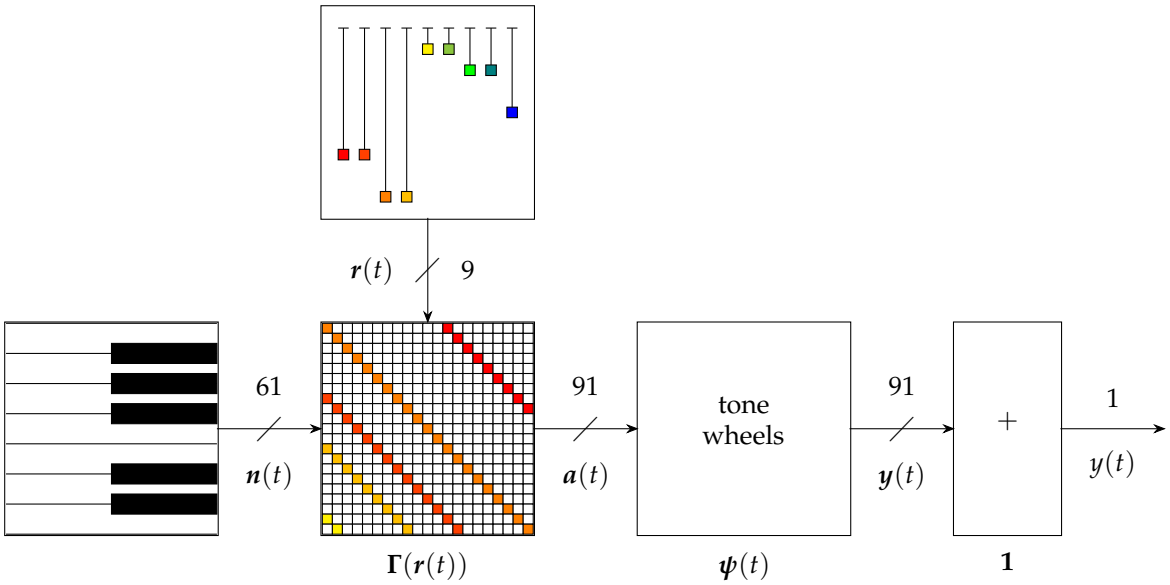

Figure 1. Hammond Tonewheel Organ block diagram.

The timbre is controlled by nine drawbars shown on the top. Each drawbar has a level $r_d(t) \in [0 \cdots 8]$ that is indexed by a drawbar number $d \in [1 \cdots 9]^\top$; these are collected into a column $\boldsymbol{r}(t)$. The drawbars may be changed over time to alter the sounds of the Hammond organ. Each drawbar's level $r_d(t)$ is converted to an amplitude in -3 dB increments (Table 2) [45].

Table 2. Amplitude of each drawbar r_d, $d \in [1 \cdots 9]$.

r_d	0	1	2	3	4	5	6	7	8
amplitude (dB)	0	-3	-6	-9	-12	-15	-18	-21	$-\infty$

Furthermore, each drawbar has a tuning offset o_d, corresponding to the tuning offset in semitones of each pseudo-harmonic. The entire set of offsets is

$$\boldsymbol{o} = [o_1 \cdots o_9]^\top = [-12, 7, 0, 12, 19, 24, 28, 31, 36]^\top \tag{1}$$

Each tuning offset (except the first two) approximates a harmonic overtone. This is discussed further at the end of the section.

Each tonewheel has a frequency f_w and amplitude $a_w(t)$ indexed by a tonewheel number $w \in [1 \cdots 91]^\top$; these are collected into columns $\boldsymbol{f}$ and $\boldsymbol{a}(t)$. Each tonewheel is tuned to the twelve-tone equal-tempered scale

$$f_w = (440)2^{(w-45)/12} \text{ Hz} \tag{2}$$

In practice there are slight deviations according to the gearing ratios, producing deviations of up to 0.69 cents [15].

The outputs of all the tonewheels are summed by the 91×1 gain block $\mathbf{1} = [1 \cdots 1]^\top$ on the right to form the output signal $y(t)$:

$$y(t) = \mathbf{1}^\top \boldsymbol{y}(t) \tag{3}$$

The 91×61 routing matrix $\boldsymbol{\Gamma}(\boldsymbol{r}(t))$ forms the 91-tall column of tonewheel amplitudes $\boldsymbol{a}(t)$ from the 61-tall column of key on/off states $\boldsymbol{n}(t)$. This is accomplished by a matrix multiply

$$\boldsymbol{a}(t) = \boldsymbol{\Gamma}(\boldsymbol{r}(t))\boldsymbol{n}(t) \tag{4}$$

$\boldsymbol{\Gamma}(\boldsymbol{r}(t))$ is sparse (most entries are 0) and has a pseudo-convolutional form [46] in which the non-zero entries $r_1(t) \cdots r_9(t) \in [0 \cdots 8]$ are dictated by the 9-tall column of drawbar levels $\boldsymbol{r}(t)$. Denoting each entry in $\boldsymbol{\Gamma}(\boldsymbol{r}(t))$ as $\gamma_{w,k}(t)$, we have

$$\gamma_{w,k}(t) = \sum_{d=1}^{9} r_d(t)\, \delta\left(w - k - o_d\right) \tag{5}$$

where $\delta(x)$ is the Kronecker delta function

$$\delta(x) = \begin{cases} 1 & , x = 0 \\ 0 & , x \neq 0 \end{cases} \tag{6}$$

The tonewheel block is comprised of 91 tonewheel processors $\psi_w(t)$ in parallel. As shown in Figure 2, each individual tonewheel processor has a tonewheel producing a periodic signal $x_w(t)$ at a particular frequency f_w, an amplitude input $a_w(t)$ provided by the routing matrix $\boldsymbol{\Gamma}(\boldsymbol{r}(t))$, and an electromagnetic model $p_w\,()$. Each tonewheel processor forms an output $y_w(t)$ by

$$y_w(t) = a_w(t)\, p_w(x_w(t)) \tag{7}$$

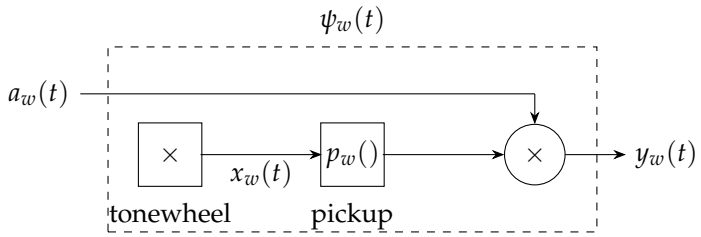

Figure 2. One tonewheel processor.

A block diagram of an individual tonewheel processor is shown in Figure 2. The matrix equation describing the entire bank of tonewheels is

$$\boldsymbol{y}(t) = \boldsymbol{p}(\boldsymbol{x}(t)) \odot \boldsymbol{a}(t) \tag{8}$$

where $\odot$ is the Hadamard (elementwise) product operator

$$(\mathbf{A} \odot \mathbf{B})_{i,j} = \mathbf{A}_{i,j}\mathbf{B}_{i,j} \tag{9}$$

where $\mathbf{A}_{i,j}$ denotes the ijth element of the matrix $\mathbf{A}$.

The lowest 12 tonewheels produce roughly square-wave signals and the rest produce essentially sinusoidal signals:

$$x_w(t) = \begin{cases} \frac{4}{\pi}\sin(2\pi\, f_w\, t) + \frac{4}{3\pi}\sin(2\pi\, 3 f_w\, t) + \frac{4}{5\pi}\sin(2\pi\, 5 f_w\, t) & , w \in [1 \cdots 12] \\ \sin(2\pi\, f_w\, t) & , w \in [13 \cdots 91] \end{cases} \tag{10}$$

As a final note, we can discuss the pseudo overtone series of the Hammond organ in more detail. Equation (5) implies a certain relationship between any pressed key k and the set of frequencies that are produced. Here we state this relationship explicitly. Given Equations (1), (2) and (5), we can see that pressing any key k will, in general, drive a set of nine tonewheels with frequencies

$$f_{k,d} = (440)2^{(k+o_d-45)/12} \quad , \quad d \in [1 \cdots 9] \tag{11}$$

Most wind and string instruments are characterized by a harmonic overtone series—i.e., one where overtone frequencies are integer multiples of a fundamental frequency. Most of the tonewheel frequencies given in Equation (11) approximate idealized harmonic overtones with frequencies given by

$$\tilde{f}_{k,d} = (440)2^{(k-45)/12}\, N_d \quad , \quad d \in [3 \cdots 9] \tag{12}$$

The first two tonewheel frequencies $f_{k,1}$ and $f_{k,2}$ are the octave below the fundamental frequency and approximately a fourth below the fundamental frequency—they are not approximations of standard harmonic overtones.

In general, $\tilde{f}_{k,d} \neq f_{k,d}$. The error in "cents" (1/100 of a semitone) is given by

$$E_d = 1200 \log_2\left(\tilde{f}_{k,d}/f_{k,d}\right) = 1200\left[o_d/12 - \log_2\left(N_d\right)\right] \quad , \quad d \in [3 \cdots 9] \tag{13}$$

The tuning error of each tonewheel frequency is independent of k; it depends only on the drawbar index d—i.e., which overtone it is supposed to be approximating. These errors are given for each drawbar in Table 1. For the fundamental and octave overtones, the tonewheels are perfectly in tune. For the 12th and 19th, the tonewheels are ≈ -1.955 cents flat of the ideal overtones. The 19th is ≈ 13.686 cents sharp. This detuning is very unique to the Hammond organ.

3. Modal Processor Review

The Hammondizer effect involves decomposing an input signal into a parallel set of narrow-band signals, analogous to a bank of organ keys. Each of the "keys" is then pitch processed according to the drawbar settings, and distortion processed according to the tonewheel and pickup mechanics and electromagnetics. It turns out that this structure closely resembles that of the modal reverberator [37,38], which forms a room response as the parallel combination of room vibrational mode responses. In the following, we review the modal reverberator and adapt it to produce the needed pitch and distortion processing.

The impulse response $h(t)$ between a pair of points in an acoustic space may be expressed as the linear combination of normal mode responses [47,48],

$$h(t) = \sum_{m=1}^{M} h_m(t) \tag{14}$$

where the system has M modes, with the mth mode response denoted by $h_m(t)$. The system output $y(t)$ in response to an input $x(t)$, the convolution $y(t) = h(t) * x(t)$, is therefore the sum of mode outputs

$$y(t) = \sum_{m=1}^{M} y_m(t), \quad y_m(t) = h_m(t) * x(t) \tag{15}$$

where the mth mode output $y_m(t)$ is the mth mode response convolved with the input. The modal reverberator simply implements this parallel combination of mode responses (15), as shown in Figure 3. Denoting by $\boldsymbol{h}(t)$ the M-tall column of complex mode responses, we have

$$y(t) = \mathbf{1}^\top (\boldsymbol{h}(t) * x(t)) \tag{16}$$

with

$$\boldsymbol{h}(t) = \boldsymbol{\psi}(t) \odot (\boldsymbol{g}(t) * \boldsymbol{\Gamma}\boldsymbol{\varphi}(t)) \tag{17}$$

and where convolution here obeys the rules of matrix multiplication, with each individual matrix operation replaced by a convolution.

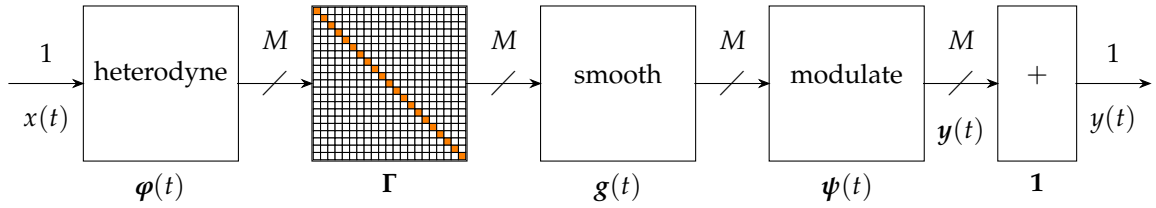

Figure 3. Basic modal reverberator architecture. The modal reverberator is the parallel combination of resonant filters matched to the modes of a linear system.

The mode responses $h_m(t)$ are complex exponentials, each characterized by a mode frequency $\omega_m = 2\pi f_w$, mode damping α_m, and mode complex amplitude γ_m,

$$h_m(t) = \gamma_m \exp\{(j\omega_m - \alpha_m)t\} \tag{18}$$

The mode frequencies and dampings are properties of the room or object; the mode amplitudes are determined by the sound source and listener positions (driver and pick-up positions for an electro-mechanical device), according to the mode spatial patterns.

Rearranging terms in the convolution $y_m(t) = h_m(t) * x(t)$, the mode filtering is seen to heterodyne the input signal to dc to form a baseband response, smooth this baseband response by convolution with an exponential, and modulate the result back to the original mode frequency,

$$y_m(t) = \sum_\tau e^{(j\omega_m - \alpha_m)(t-\tau)} x(\tau) = e^{j\omega_m t} \sum_\tau \gamma_m e^{-\alpha_m(t-\tau)} \left[e^{-j\omega_m \tau} x(\tau) \right] \tag{19}$$

All M γs are stacked into a diagonal gain matrix $\boldsymbol{\Gamma}$. All the heterodyning sinusoids are stacked into a column $\boldsymbol{\varphi}(t)$, and all of the modulating sinusoids into a column $\boldsymbol{\psi}(t)$. The mode damping filters are stacked into a column $\boldsymbol{g}(t)$. This process is shown in Figure 4. The heterodyning and modulation steps implement the mode frequency, and the smoothing filter generates the mode envelope, an exponential decay.

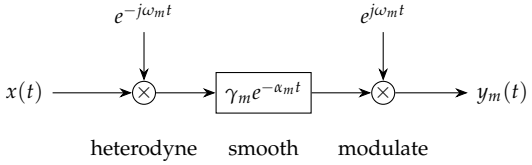

Figure 4. Mode response implementation. The mode response may be implemented as a cascade of heterodyning, smoothing, and modulation operations.

Using this architecture, rooms and objects may be simulated by tuning the filter resonant frequencies and dampings to the corresponding room or object mode frequencies and decay times.

The parallel structure allows the mode parameters to be separately adjusted, while Equation (19) provides interactive parameter control with no computational latency.

As described in [39], the modal reverberator architecture can be adapted to produce pitch shifting by using different sinusoid frequencies for the heterodyning and modulation steps in Equation (19), and adapted to produce distortion effects by inserting nonlinearities on the output of each mode or group of modes. The modal processor architecture has been used for other effects, including mode-wise gated reverb using Truncated Infinite Impulse Response (TIIR) filters [49], groupwise distortion, time stretching by resampling of the baseband signals, and manipulation of mode time envelopes by introducing repeated poles [39].

4. Hammondizer Modal Processor Implementation

The Hammondizer effect system architecture is shown in Figure 5. It turns out that this structure closely resembles that of the modal reverberator (Figure 3), which forms a room response as the parallel combination of room vibrational mode responses. Both have inputs designated by $x(t)$, a column of narrow-band outputs designated by $\boldsymbol{y}(t)$, summed to form the system output $y(t)$.

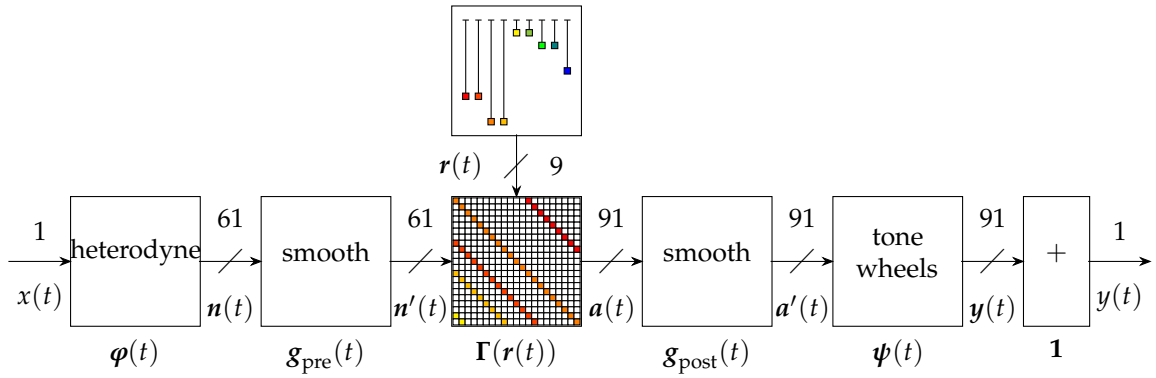

Figure 5. Block diagram of the Hammondizer effect.

In the Hammondizer, the input signal $x(t)$ is heterodyned to baseband by a column of modulating sinusoids $\boldsymbol{\varphi}(t)$:

$$\boldsymbol{n}(t) = \boldsymbol{\varphi}(t)x(t) \tag{20}$$

These baseband signals are smoothed by a column of pre-smoothing filters $\boldsymbol{g}_{\text{pre}}(t)$

$$\boldsymbol{n}'(t) = \boldsymbol{g}_{\text{pre}}(t) * \boldsymbol{n}(t) \tag{21}$$

A column of tonewheel amplitudes $\boldsymbol{a}(t)$ is formed by the drawbar routing matrix $\boldsymbol{\Gamma}(\boldsymbol{r}(t))$,

$$\boldsymbol{a}(t) = \boldsymbol{\Gamma}(\boldsymbol{r}(t))\boldsymbol{n}'(t) \tag{22}$$

and further smoothed by a column of post-smoothing filters $\boldsymbol{g}_{\text{post}}(t)$:

$$\boldsymbol{a}'(t) = \boldsymbol{g}_{\text{post}}(t) * \boldsymbol{a}(t) \tag{23}$$

A set of mode outputs $\boldsymbol{y}(t)$ is formed by the tonewheel processing stages $\boldsymbol{\psi}(t)$, which include a column of pickup models $\boldsymbol{p}()$ and modulating signals $\boldsymbol{x}(t)$

$$\boldsymbol{y}(t) = \boldsymbol{p}\left(\boldsymbol{x}(t) \odot \boldsymbol{a}'(t)\right) \tag{24}$$

An individual tonewheel processing stage is shown in Figure 6. Notice the slight change in architecture from the analogous Figure 2. In Figure 6, the pickup distortion has been moved to

operate on the output rather than the raw tonewheel signal. The reason for this change is artistic—it disambiguates the effects of the memoryless pickup nonlinearities and the distortion of the tonewheel basis functions.

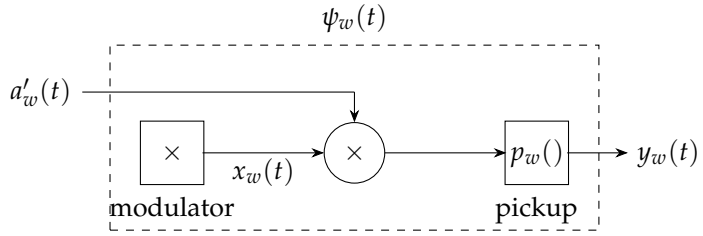

Figure 6. One tonewheel processor in the Hammondizer.

Finally, the output $y(t)$ is formed by summing all of the mode outputs:

$$y(t) = \mathbf{1}^\top \boldsymbol{y}(t) \tag{25}$$

In the rest of this section, we describe in detail how aspects of the modal processor are tuned and adapted to create the Hammondizer. Pitch processing adaptations include tuning the modes to the particular frequencies and frequency range of the Hammond organ Section 4.1), introducing drawbar-style controls to pitch processing (Section 4.2), adding vibrato to mode frequencies (Section 4.3), and adding crosstalk between nearby modes to simulate crosstalk between nearby tonewheels (Section 4.4). Distortion processing adaptations include adapting saturating nonlinearities for each mode to mimic the pickup distortion of each tonewheel (Section 4.5) and replacing modulation sinusoids with sums of sinusoids to mimic non-sinusoidal tonewheel shapes (Section 4.6).

4.1. Frequency Range

The first step of adapting the modal reverberator to create the Hammondizer effect is to pick the mode frequencies which specify the heterodyning and modulating sinusoids $\boldsymbol{\varphi}(t)$ and $\boldsymbol{\psi}(t)$. The unique sound of the Hammond organ is largely due to the tonewheels being tuned to the 12-tone equal tempered scale. Here we discuss how to preserve this feature in the context of the Hammondizer audio effect.

Since each mode of the modal reverberator is a narrow bandpass filter, a sufficient frequency density of modes is required to support typical wideband musical signals. In particular, unless each frequency component of the input is sufficiently close to a mode center, it may not contribute audibly to the output. For this reason, tuning the modal reverberator's frequencies to the 12-tone equal tempered scale used by the Hammond organ heavily attenuates the frequencies "in the cracks", producing an artificial sound (compare to composer Peter Ablinger's "Talking Piano" [50]).

To avoid this effect, we use many exponentially-spaced mode frequencies per semitone. Denoting the number of modes per semitone as S, the tuning of each mode is

$$f_w = f_1 \, 2^{w/(12\,S)} \text{ Hz} \tag{26}$$

(cf. Equation (2)). S is chosen to satisfy two subjective constraints. As S gets larger, the computational cost of the modal processor grows. As S becomes small, the modal density decreases and produces an artificial sound. We found by experimentation that $S = 14$ is a good setting that balances these two constraints.

Heterodyning and modulating sinusoids at constant frequencies are given by

$$\varphi_w(t) = \exp\{-j\omega_w t\} \tag{27}$$

$$\psi_w(t) = \exp\{+j\omega_w t\} \tag{28}$$

(cf. Equation (18)).

The next step of adapting the modal reverberator to create the Hammondizer effect is to choose the range of mode frequencies. The range of the Hammond organ is C1 (≈32.7 Hz) to F#7 (≈5919.9 Hz). For simplicity, we set $f_1 = 40$ Hz and let the modes range up seven octaves, up to $f_{1177} = 5120$ Hz; these modes are indexed by a tonewheel index $w \in [1 \cdots 1177]$. These round numbers correspond very closely to the range of the Hammond organ. Forty Hz corresponds to $k \approx 3.5$ and 5120 Hz to $k \approx 87.5$; therefore, this range technically cuts off ≈3 semitones from the top and bottom of the range of the Hammond organ tonewheel range. Nonetheless, it does not negatively affect the qualitative effect of the Hammondizer.

4.2. Tone Controls

The heart of the Hammondizer effect is the drawbar tone controls. As before, the drawbar settings give a column $\boldsymbol{r}(t)$ of registrations, which drive the entries of the sparse matrix $\boldsymbol{\Gamma}(\boldsymbol{r}(t))$ according to

$$\gamma_{w,k}(t) = \sum_{d=1}^{9} r_d(t)\, \delta\left(w - k - o_d\, S\right) \tag{29}$$

The only difference from Equation (5) is the presence of S to account for the multiple modes per semitone.

In the Hammondizer context, the entries in $\boldsymbol{\Gamma}(\boldsymbol{r}(t))$ control a Hammond-style pitch shift. The structure of $\boldsymbol{\Gamma}(\boldsymbol{r}(t))$ means that energy in a smoothed baseband signal $n_w(t)$ (centered at some mode frequency f_w) contributes to *nine* different tonewheel amplitudes f_κ, $\kappa \in \mathbf{1}w + S\boldsymbol{o}$, according to $\gamma_{w,\kappa}(t)$.

4.3. Vibrato

A vibrato effect that can mimic Hammond organ vibrato is created when the frequencies of the modulating sinusoids $\boldsymbol{\psi}(t)$ are varied. In this case, modulation sinusoids can be implemented with phase accumulators

$$x_w(t) = \exp\{-j\theta_w(t)\} \tag{30}$$

Each vibrato phase signal is given by

$$\theta_w(t) = \theta_w(t-1) + 2^{V_{\text{depth}}/1200 \sin(2\pi/f_s\, V_{\text{rate}} t)} 2\pi/f_s \tag{31}$$

where V_{depth} is the vibrato depth in cents and V_{rate} is the vibrato rate in Hz.

An early Hammond patent [20] praises "…a musical tone containing a vibrato, that is, a cyclical shift in frequency of approximately 1.5%, at a rate of about 6 per second…" To match that design criteria, we typically choose a vibrato depth of 26 cents ≈1.5% and a vibrato rate of 6 Hz. Of course, these can be parameterized as desired.

4.4. Crosstalk

Some aficionados point to crosstalk between tonewheels as an important part of Hammond organ sonics. We can consider that since mode filters are not "brick wall" filters, there is already a sort of crosstalk built into the Hammondizer effect.

Drawing inspiration from Pekonen et al. [18], we can explicitly simulate leakage between adjacent tonewheels by adding another matrix multiply between $\boldsymbol{g}_{\text{post}}(t)$ and $\boldsymbol{\psi}(t)$. This creates a new set of signals with crosstalk that includes modes one semitone away from the main modes with a crosstalk level C:

$$a''_w(t) = Ca'_{w-S}(t) + a'_w(t) + Ca'_{w+S}(t) \tag{32}$$

4.5. Memoryless Pickup Nonlinearities

As detailed in [39], distortion effects may be generated by passing a mode through a memoryless nonlinear function or by substituting a complex waveform for the modulation sinusoid waveform. Here we adapt both types of distortion to mimic aspects of the Hammond organ's sonics and design to the Hammondizer. Note that since both kinds of distortion are applied separately to each mode, the output will contain no intermodulation products.

Drawing inspiration from the Mustonen et al.'s model of a guitar pickup [10], we propose a memoryless nonlinearity of the form

$$y_w(t) = \left(1 - e^{-\alpha x_w(t) a'_w(t)}\right) / \alpha \tag{33}$$

This memoryless nonlinearity is shown for values of $\alpha \in [0.1, 0.3, 0.9]$ in Figure 7. This has the property of maintaining unity gain around zero, but distorting signals with a large swing around zero by compressing positive signals and expanding negative signals. In this article, we will use a value of $\alpha = 0.3$.

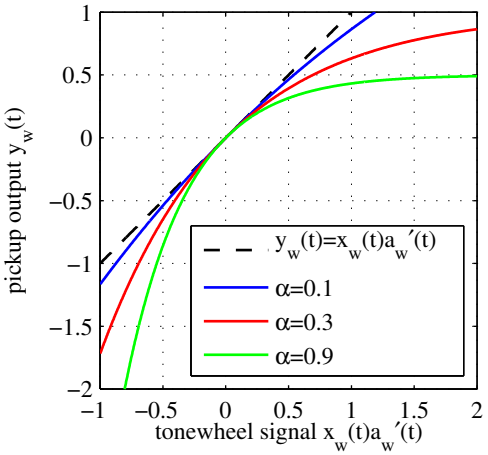

Figure 7. Memoryless tonewheel pickup nonlinearity.

Typically, memoryless nonlinearities like this will produce effects including "harmonic distortion" (new frequencies at multiples of existing frequencies) and "intermodulation products" (new frequencies at sums and differences of existing frequencies). Since this memoryless nonlinearity is applied to the output of a bandpass filter, mostly harmonic distortion will be created, since energy is concentrated at one frequency.

4.6. Tonewheel Basis Distortion

On the Hammond organ, tonewheels may not be perfectly sinusoidal. Also, the lowest octave of tonewheels are cut closer to a square wave shape than a sinusoid. This can be considered a distortion of the sinusoidal basis functions that the tonewheels represent. To approximate this distortion of the lower tonewheel basis functions, we can replace each modulating sinusoid $\psi_w(t)$ with a *sum* of sinusoids

$$\tilde{\psi}_w(t) = \frac{4}{\pi}\exp(jw_w\, t) + \frac{4}{3\pi}\exp(j3f_w\, t) + \frac{4}{5\pi}\exp(j5f_w\, t) \tag{34}$$

(cf. Equation (10)).

Drawing inspiration from the Hammond organ, this should be done for the lowest octave of tonewheels. In practice, it can be useful to define the effect for a large range of modes.

Note that this distortion is very different in character from the saturating nonlinearities. Specifically, it has the unique feature of being amplitude-independent.

5. Results and Discussion

To demonstrate the features of the Hammondizer, we present a series of examples. Examples of the pitch processing and distortion processing Hammondizer components, operating on a pure tone input, are presented in Sections 5.1 and 5.2, respectively. Examples of the full Hammondizer, applied to program material, are described in Section 5.3. Aspects of the Hammondizer's sonics are visible in the spectrogram and explained in the text. To understand the full effect of the Hammondizer, it is necessary to listen to it. Audio recordings (.wav file format) of all these examples are available online [51].

For all of these examples, the Hammondizer is configured to have 1177 exponentially spaced modes, with 14 modes per semitone over the seven octave range from 40 Hz to 5120 Hz. The two columns of smoothing operations $g_{\text{pre}}(t)$ and $g_{\text{post}}(t)$ are set so that the gain of each mode during the smoothing operations is set to unity. $g_{\text{pre}}(t)$ is simply a column of ones. Except where noted, each mode is assigned a 200-ms decay time. We form $g_{\text{post}}(t)$ using smoothing filters which are applied twice, as suggested in [39]. This creates impulse responses with a linear ramp onset and a 200-ms decay (e.g., [52])—i.e., of the form $t \exp\{-\alpha t\}$.

Although we have not emphasized the variation of the mode dampings and complex amplitudes in this article—focusing rather on the novel aspects of the Hammondizer—the mode dampings and complex amplitudes can be set just as in the modal reverberator [37,38], creating hybrid Hammond/reverb effects. The different Hammond organ registrations shown in these results are given in Figure 8 and are taken from a Hammond owner's manual [53] and a Keyboard Magazine article [54].

5.1. Pitch Processing Examples

In this section, we demonstrate the Hammondizer's drawbar tone controls (Figure 9), its frequency range (Figure 10), and crosstalk and vibrato processing (Figure 11).

Figure 9 shows spectrograms of a pure tone input signal and versions processed with the Hammondizer. The input signal (Figure 9a) is a 1.75-second-long sine wave tuned to middle C (C3, ≈261.63 Hz). The output signal (Figure 9b) shows five different Hammondized versions of the input signal. Each of the five versions uses a different registration; the vibrato, crosstalk, and distortion were disabled. The different Hammond organ registrations shown in these results are given in Figure 8. Figure 9b uses the first five registrations of Figure 8 in order.

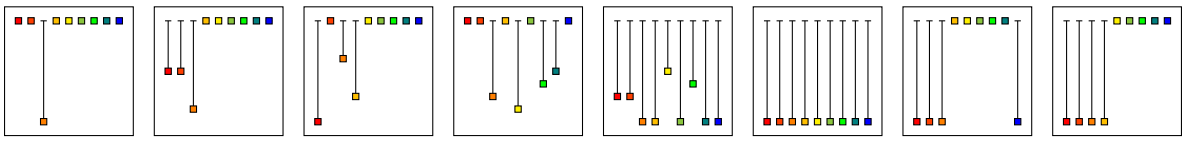

Figure 8. Various Hammond organ registrations and their names. (**a**) 008000000 fundamental; (**b**) 447000000 "bassoon"; (**c**) 803600000 "mellow-Dee"; (**d**) 006070540 "clarinet"; (**e**) 668848588 "shoutin' "; (**f**) 888888888 "all out"; (**g**) 888000008 "whistle stop"; (**h**) 888800000 "Jimmy Smith".

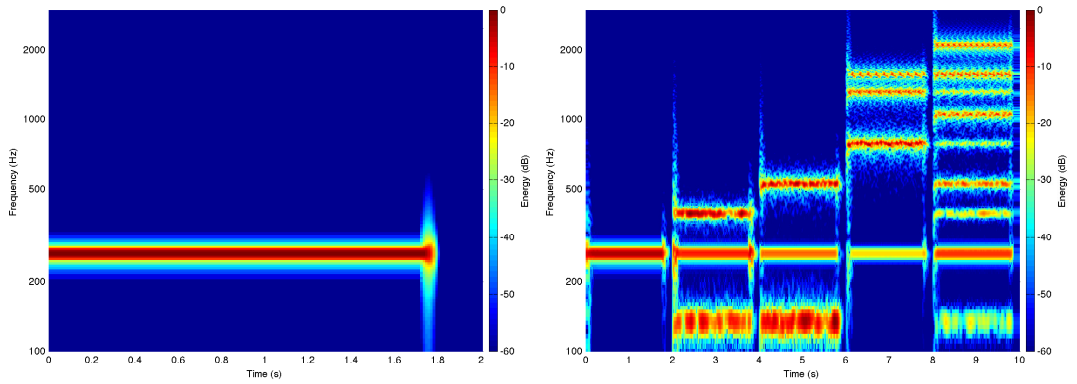

Figure 9. (**a**) C3 sine wave input and (**b**) Hammondized version with five different registrations.

The C3 sine wave is tuned very close to the center frequency of mode $w = 455$. Knowing that the Hammondizer uses the matrix $\mathbf{\Gamma}(\boldsymbol{r}(t))$ to drive output modes that are offset from each analysis mode by the length-9 column $\boldsymbol{o}$ (recall Table 1 and Equation (1)), we expect that an input consisting of a single sinusoid will in general create output signals with nine sinusoidal components (recall Equation (11)) near modes $(287, 553, 455, 623, 721, 791, 847, 889, 959)$. However, since $\mathbf{\Gamma}(\boldsymbol{r}(t))$ is a function of the registration $\boldsymbol{r}(t)$, the output behavior is heavily dependent on the registration. Notice that the 008000000 registration does not affect the signal much beyond a slight lengthening due to the decay time of the modes near C3. Since each $r(t)$ except $r_3(t)$ is zero, only one sinusoid comes out. The second setting, "bassoon" (447000000) produces three sinusoids in response to the input sinusoid, since it has three non-zero $r(t)$s. The amplitude of each sinusoid depends on its corresponding drawbar setting (recall Table 2). The "bassoon," "mellow-Dee," and "shoutin' " registrations have non-zero first drawbar settings—notice that they produce energy an octave below C3. The "shoutin' " and "all out" registrations have no non-zero drawbar settings—notice that the individual sine wave of the input has driven nine sine waves in the output, and that their relative amplitudes reflect the "shoutin' " and "all out" registrations (668848588 and 888888888, respectively).

Figure 10 shows spectrograms of a sinusoidal input signal and its Hammondized response. The input signal (Figure 10a) is a series of nine 0.5-second-long sine waves, generated at octave intervals from C0 (≈32.70 Hz) and to C8 (≈8372.02 Hz). The Hammondized output (Figure 10a) used the 668848588 ("shoutin' ") registration, and the vibrato, crosstalk, and distortion were disabled. In a broad sense, the Hammondizer imprints the "shoutin' " partial structure onto the input sinusoids. Note, however, that since the Hammondizer does not have any modes outside the 40 Hz to 5120 Hz frequency range, the C0 and C8 inputs generate little output, though transients in the C0 sinusoid produce a ghostly "whoosh" sound.

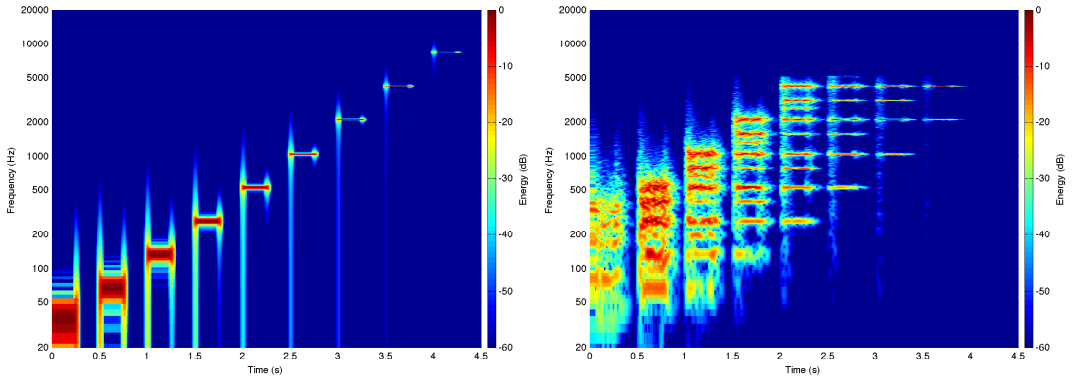

Figure 10. Showing range of Hammond tonewheels. (**a**) C0–C8 input signal; (**b**) Hammondizer with "shoutin' " registration.

The Hammondizer crosstalk and vibrato components are now explored using the pure tone input of Figure 9a. In Figure 11a, the effect of crosstalk is illustrated using the "clarinet" registration with vibrato and distortion disabled. Crosstalk amplitudes of $-\infty$, -24, -18, -12, and -6 dB are simulated. Note the increased presence of energy in adjacent notes with increased crosstalk amplitude. In Figure 11b, the effect of vibrato is studied using a "whistle stop" (888000008) registration, with crosstalk and distortion disabled. Each output uses a 6 Hz vibrato, with (from left to right) vibrato depths of 0, 25, 50, 100, and 1200 cents, with a depth of 25 cents being typical for a Hammond tonewheel organ. As expected, there is a sinusoidal variation in the output frequency of each partial.

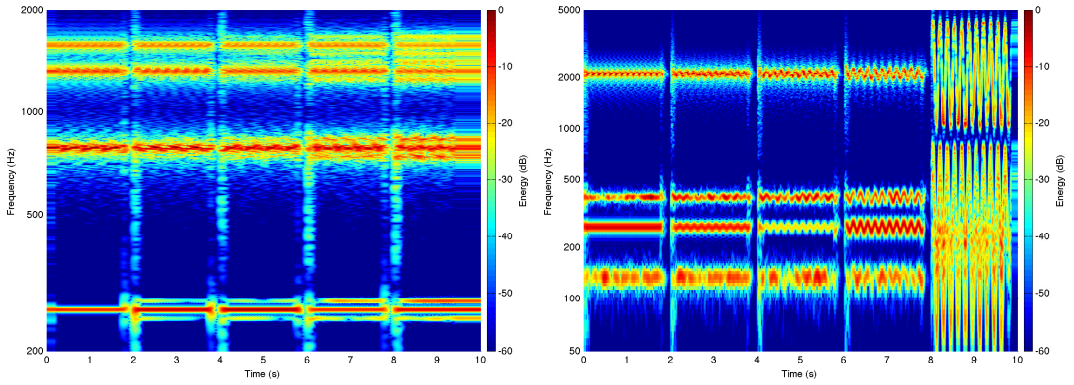

Figure 11. (**a**) Clarinet registration, various levels of crosstalk $\in [-\infty, -24, -18, -12, -6]$ dB and (**b**) Whistle stop registration, various levels of vibrato $\in [0, 26, 50, 100, 1200]$ cents on the right.

5.2. Distortion Processing Examples

Here, we demonstrate the Hammondizer's tonewheel shape distortion (Figure 12) and its mode-wise distortion (Figures 13 and 14).

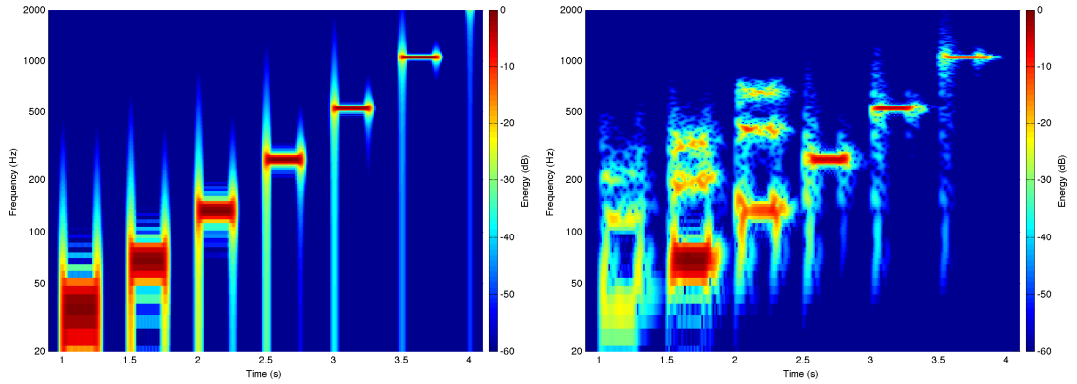

Figure 12. Keyboard split demonstration. (**a**) C0–C5 input signal; (**b**) Driving keyboard split.

Figure 12 shows an input signal spectrogram (Figure 12a) and a Hammondized version showing the tonewheel shape distortion (Figure 12b). The input signal is the collection of sinusoids C0 through C5. This is applied to the Hammondizer set to a fundamental-only registration (008000000), with vibrato and distortion disabled. As described above, the lowest two octaves of tonewheels are given 3rd and 5th harmonics. Notice how C0, C1, and C2 produce pronounced 3rd and 5th harmonics even though the registration is 008000000, but that C3–C5 don't generate harmonics.

Figure 13 shows spectrograms of an input signal and its Hammondized version. Figure 13a shows the input signal: five 1.75-second-long sinusoidal bursts, all tuned to C3. From left to right, the input sinusoid amplitudes are 0, -3, -6, -9, and -12 dB. Notice in the output (Figure 13b) that the degree of distortion decreases as the amplitude decreases, as is typical of saturating memoryless nonlinearities.

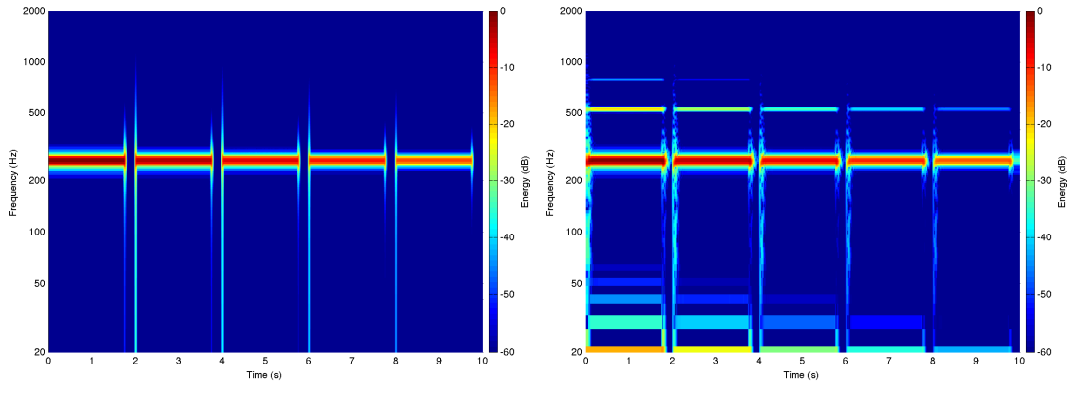

Figure 13. Decreasing amplitude interacting with distortion. (**a**) C3 input signal, various amplitudes; (**b**) Distorted.

Recall that the Hammond distortion is generated separately on each key, and accordingly there is no intermodulation distortion. To demonstrate this and to test the presence of intermodulation distortion in our Hammondizer process, we use a signal having C3 and E3 notes which appear both individually and overlapped—see Figure 14. Figure 14b shows the Hammondized result. Notice that there is little to no intermodulation distortion in the output; the response to the combination of C3 and E3 is very nearly equal to the sum of the response to C3 and the response to E3. Figure 14c shows the result of a modified algorithm $y(t) = p(\mathbf{1}^\top(\boldsymbol{x}(t) \odot \boldsymbol{a}'(t)))$ in which the hundreds of individual mode pickup distortions are replaced by a single pickup distortion that operates on the sum of all modes.

(cf. Equations (24) and (25)). This more typical approach to implementing distortion produces heavy intermodulation distortion. This sort of intermodulation distortion can be considered unpleasant; its absence can be considered a unique feature of the Hammondizer.

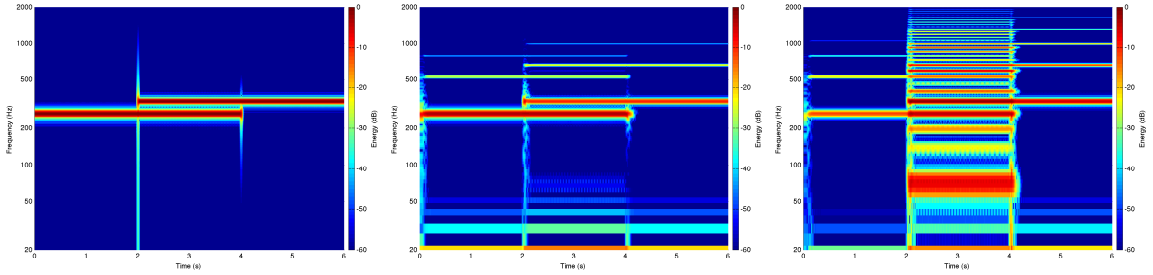

(a) (b) (c)

Figure 14. Showing how the Hammondizer mode-wise distortion does not cause intermodulation distortion. (**a**) Input signal; (**b**) Hammondizer with mode-wise distortion; and (**c**) Hammondizer with "global" distortion.

5.3. Full Examples

In this section, we present examples of the full Hammondizer processing program material, a guitar (Figure 15) and a violoncello (Figure 16).

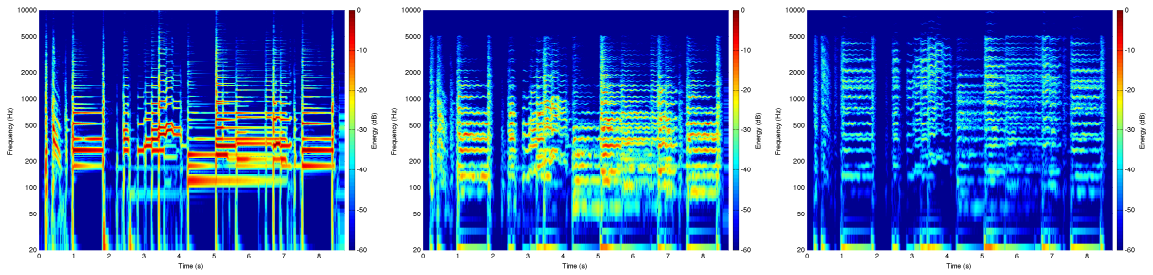

(a) (b) (c)

Figure 15. Blues guitar lick, original and two different Hammondized settings. (**a**) Input signal; (**b**) Hammondized, "Jimmy Smith" registration; (**c**) Hammondized, "all out" registration.

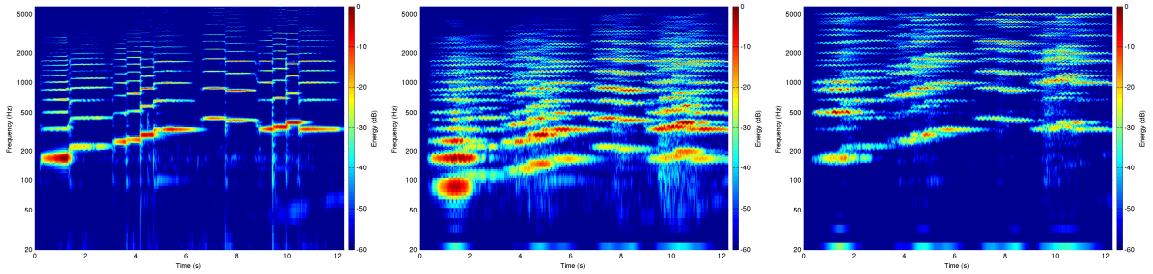

(a) (b) (c)

Figure 16. Beginning of "El Cant dels Ocells" [55], original and two different Hammondized settings. (**a**) Input signal; (**b**) Hammondized, "bassoon" registration; (**c**) Hammondized, "clarinet" registration.

Figure 15a shows a blues guitar lick, and two Hammondized versions, with a "Jimmy Smith" (888800000) registration in Figure 15b and an "all out" (888800000) registration in Figure 15c. Notice that

the relatively full-range input of the guitar is mostly restricted to below 5120 Hz in the Hammondized examples. Especially from 1–2 s, the vibrato is visible. In the "all out" registration, some pickup distortion is visible above the 5120-Hz tonewheel limit.

Figure 16a shows a melody "El Cant dels Ocells" played on the violoncello, and two Hammondized versions, with a "bassoon" (447000000) registration in Figure 16b and a "clarinet" (006070540) registration in Figure 16c.

6. Conclusions

In this article, we've described a novel class of audio effects—the Hammondizer—that imprints the sonics of the Hammond tonewheel organ on any audio signal. The Hammondizer extends the recently-introduced modal processor approach to artificial reverberation and effects processing. We close with comments on two extensions to the Hammondizer audio effect.

We've discussed parameterizations of each aspect of the Hammondizer which are chosen to closely mimic the sonics of the Hammond organ. For example, the mode frequency range of the Hammondizer is chosen to match the range of tonewheel tunings on the Hammond organ, and the the vibrato rate and depth are chosen to mimic a standard Hammond organ vibrato tone. In closing, we wish to mention that these parameterizations can be extended to loosen the connection to the Hammond organ but widen the range of applicability of the Hammondizer. For instance, the mode frequencies can be tuned across the entire audio range (≈20–20000 Hz) rather than being limited to 40–5120 Hz. In this context, some of the connection with the Hammond organ is relaxed, but the drawbar controls still give a powerful and unique interface for pitch shift in a reverberant context.

Although the Hammondizer is designed to process complex program material as a digital audio effect, it is possible to configure the Hammondizer so that it will act somewhat like a direct Hammond organ emulation. This can be done by driving the Hammondizer with only sinusoids (e.g., a keyboard set to a sinusoid tone) which act as control signals, effectively driving $\boldsymbol{n}(t)$ directly. This is particularly effective using short mode dampings (as in this article). An example is given alongside the other audio online [51].

Acknowledgments: Thanks to Ross Dunkel for discussions on the Hammond Organ.

Author Contributions: Kurt James Werner drafted the main manuscript and helped write signal processing code. Jonathan S. Abel supervised the research, helped in the preparation of the manuscript, and wrote the signal processing code.

Conflicts of Interest: The authors declare no conflict of interest.

References

1. Hammond, L. Electrical Musical Instrument. U.S. Patent 1,956,350, 24 April 1934.
2. Ng, T.K. *The Heritage of the Future: Historical Keyboards, Technology, and Modernism*. Ph.D Thesis, University of California, Berkeley, CA, USA, 2015.
3. Faragher, S. *The Hammond Organ: An Introduction to the Instrument and the Players Who Made It Famous*; Hal Leonard Books: Milwaukee, WI, USA, 2011.
4. Smith, J.O., III. Spectral Audio Signal Processing. Additive Synthesis (Early Sinusoidal Modeling). 2011. Available online: https://ccrma.stanford.edu/~jos/sasp/Additive_Synthesis_Early_Sinusoidal.html (accessed on 21 March 2016).
5. Bode, H. History of electronic sound modification. *J. Audio Eng. Soc. (JAES)* **1984**, *32*, 730–739.
6. Ebeling, K.; Freudenstein, K.; Alrutz, H. Experimental investigation of statistical properties of diffuse sound fields in reverberation rooms. *Acta Acust. United Acust.* **1982**, *51*, 145–153.
7. Jungmann, T. Theoretical and Practical Studies on the Behaviour of Electric Guitar Pickups. Diploma Thesis, Helsinki University of Technology, Helsinki, Finland, November 1994.
8. Remaggi, L.; Gabrielli, L.; de Paiva, R.C.D.; Välimäki, V.; Squartini, S. A pickup model for the Clavinet. In Proceedings of the 15th International Conference on Digital Audio Effects (DAFx-12), York, UK, 17–21 September 2012.

9. Gabrielli, L.;Välimäki, V.; Penttinen, H.; Squartini, S.; Bilbao, S. A digital waveguide-based approach for Clavinet modeling and synthesis. *EURASIP J . Adv. Signal Process.* **2013**, *2013*, 103, doi:10.1186/1687-6180-2013-103.
10. Mustonen, M.; Kartofelev, D.; Stulov, A.; Välimäki, V. Experimental verification of pickup nonlinearity. In Proceedings of the International Symposium on Musical Acoustics (ISMA), Le Mans, France, 7–12 July 2014; pp. 651–656.
11. Thornburg, H. Antialiasing for nonlinearities: Acoustic modeling and synthesis applications. In Proceedings of the International Computer Music Conference (ICMC), Beijing, China, 22–27 October 1999.
12. Horton, N.G.; Moore, T.R. Modeling the magnetic pickup of an electric guitar. *Am. J. Phys.* **2009**, *77*, 144–150.
13. Paiva, R.C.D.; Pakarinen, J.; Välimäki, V. Acoustics and modeling of pickups. *J. Audio Eng. Soc. (JAES) 2012*, *60*, 768–782.
14. Esqueda, F.; Välimäki, V.; Bilbao, S. Aliasing reduction in soft-clipping algorithms. In Proceedings of the 23rd European Signal Processing Conference (EUSIPCO), Nice, France, 31 August–4 September 2015; pp. 2059–2063.
15. Wiltshire, T. Technical aspects of the Hammond Organ. Available online: http://electricdruid.net/technical-aspects-of-the-hammond-organ/ (accessed on 21 March 2016)
16. Hammond Tone Wheels. Available online: http://www.goodeveca.net/RotorOrgan/ToneWheelSpec.html/ (accessed on 21 March 2016)
17. Reid, G. *Synthesizing Hammond Organ Effects: Part 1*; Sound on Sound (SOS): Cambridge, UK, January 2004.
18. Pekonen, J.; Pihlajamäki, T.; Välimäki, V. Computationally efficient Hammond organ synthesis. In Proceedings of the 14th International Conference on Digital Audio Effects (DAFx-11), Paris, France, 19–23 September 2011.
19. An Introducion to Drawbars. Available online: http://www.hammond-organ.com/product_support/drawbars.htm (accessed on 21 March 2016).
20. Hanert, J.M. Electrical musical apparatus. U.S. Patent 2,382,413, 14 August 1945.
21. Leslie, D.J. Rotatable Tremulant Sound Producer. U.S. Patent 2,489,653, 29 November 1949.
22. Meinema, H.E.; Johnson, H.A.; Laube, W.C., Jr. A new reverberation device for high fidelity systems. *J. Audio Eng. Soc. (JAES)* **1961**, *9*, 284–326,
23. Smith, J.; Serafin, S.; Abel, J.; Berners, D. Doppler simulation and the Leslie. In Proceedings of the 5th International Conference on Digital Audio Effects (DAFx-02), Hamburg, Germany, 26–28 September 2002.
24. Smith, J.O, III. Physical Audio Signal Processing for Virtual Musical Instruments and Audio Effects. The Leslie. 2010. Available online: https://ccrma.stanford.edu/~jos/pasp/Leslie.html (accessed on 21 March 2016).
25. Disch, S.; Zölzer, U. Modulation and delay line based digital audio effects. In Proceedings of the 2nd COST G-6 Workshop on Digital Audio Effects (DAFx-99), Trondheim, Norway, 9–11 December 1999.
26. Dutilleux, P.; Holters, M.; Disch, S.; Zölzer, U. Modulators and Demodulators. In *DAFX: Digital Audio Effects*, 2nd ed.; John Wiley & Sons: West Sussex, UK, 2011; pp. 83–99.
27. Zölzer, U. *DAFX: Digital Audio Effects*, 2nd ed.; John Wiley & Sons: West Sussex, UK, 2011.
28. Kronland-Martinet, R.; Voinier, T. Real-time perceptual simulation of moving sources: Application to the Leslie cabinet and 3D sound immersion. *EURASIP J. Audio Speech Music Process.* **2008**, *2008*, 849696, doi:10.1155/2008/849696.
29. Herrera, J.; Hanson, C.; Abel, J.S. Discrete time emulation of the Leslie speaker. In Proceedings of the 127th Convention of the Audio Engineering Society (AES), New York, NY, USA, 9–12 October 2009.
30. Välimäki, V.; Abel, J.S.; Smith, J.O. Spectral delay filters. *J. Audio Eng. Soc. (JAES)* **2009**, *57*, 521–531.
31. Werner, K.J.; Dunkel, W.R.; Germain, F.G. A computational model of the Hammond organ vibrato/chorus using wave digital filters. In Proceedings of the 19th International Conference on Digital Audio Effects (DAFx-16), Brno, Czech, 5–9 September 2016.
32. Reid, G. *Synthesizing Tonewheel Organs*; Sound on Sound (SOS): Cambridge, UK, November 2003.
33. Reid, G. *Synthesizing Tonewheel Organs: Part 2*; Sound on Sound (SOS): Cambridge, UK, December 2003.
34. Reid, G. *Synthesizing the Rest of the Hammond Organ: Part 2*; Sound on Sound (SOS): Cambridge, UK, February 2004.
35. Reid, G. *Synthesizing the Rest of the Hammond Organ: Part 3*; Sound on Sound (SOS): Cambridge, UK, March 2004.

36. Pakarinen, J.; Välimäki, V.; Fontana, F.; Lazzarini, V.; Abel, J.S. Recent advances in real-time musical effects, synthesis, and virtual analog models. *EURASIP J. Adv. Signal Process.* 2011, *2011*, 940784, doi:10.1155/2011/940784.
37. Abel, J.S.; Coffin, S.; Spratt, K.S. A modal architecture for artificial reverberation. *J. Acoust. Soc. Am.* **2013**, *134*, 4220, doi:10.1121/1.4831495.
38. Abel, J.S.; Coffin, S.; Spratt, K.S. A modal architecture for artificial reverberation with application to room acoustics modeling. In Proceedings of the 137th Convention of the Audio Engineering Society (AES), Los Angeles, CA, USA, 9–12 October 2014.
39. Abel, J.S.; Werner, K.J. Distortion and pitch processing using a modal reverb architecture. In Proceeding of the 18th International Conference on Digital Audio Effects (DAFx-15), Trondheim, Norway, 30 November–3 December 2015.
40. Välimäki, V.; Parker, J.D.; Savioja, L.; Smith, J.O.; Abel, J.S. More than fifty years of artificial reverberation. In Proceedings of the 60th International Conference of the Audio Engineering Society (AES), Leuven, Belgium, 3–5 February 2016.
41. Bilbao, S. Sound synthesis and physical modeling. In *Numerical Sound Synthesis*; Wiley: Hoboken, NJ, USA, 2009.
42. Avanzini, F.; Marogna, R. A modular physically based approach to the sound synthesis of membrane percussion instruments. *IEEE Trans. Audio Speech Lang. Process.* **2010**, *18*, 891–902.
43. Morrison, J.D.; Adrien, J.-M. MOSAIC: A framework for modal synthesis. *Comput. Music J.* **1993**, *17*, 45–56.
44. Trautmann, L.; Rabenstein, R. Classical synthesis methods based on physical models. In *Digital Sound Synthesis by Physical Modeling Using the Functional Transform Method*, 1st ed.; Springer: New York, NY, USA, 2003.
45. Vorkoetter, S. The Science of Hammond Organ Drawbar Registration. Available online: http://www.stefanv.com/electronics/hammond_drawbar_science.html (accessed on 21 March 2016).
46. Smith, J.O., III. Mathematics of the Discrete Fourier Transform (DFT) with Audio Applications. Convolution. 2007. Available online: https://ccrma.stanford.edu/~jos/mdft/Convolution.html (accessed on 21 March 2016).
47. Morse, P.M.; Ingard, K.U. *Theoretical Acoustics*; Princeton University Press: Princeton, NJ, USA, 1987.
48. Fletcher, N.H.; Rossing, T.D. *Physics of Musical Instruments*, 2nd ed.; Springer: Berlin, Germany, 2010.
49. Wang, A.; Smith, J.O. On fast FIR filters implemented as tail-canceling IIR filters. *IEEE Trans. Signal Process.* **1997**, *45*, 1415–1427.
50. Barrett, G.D. Between noise and language: The sound installations and music of Peter Ablinger. *Mosaic J. Interdiscip. Study Lit.* **2009**, *42*, 147–164.
51. Werner, K.J.; Abel, J.S. "Modal Processor Effects Inspired by Hammond Tonewheel Organs"—Audio Examples. Available online: https://ccrma.stanford.edu/~kwerner/appliedsciences/hammondizer.html (accessed on 20 June 2016).
52. Abel, J.S.; Wilson, M.J. Luciverb: Iterated convolution for the impatient. In Proceedings of the 133rd Convention of the Audio Engineering Society (AES), San Francisco, CA, USA, 26–29 October 2012.
53. Hammond Suzuki, Ltd. Model: Sk1/ Sk2 stage keyboard owner's manual. Document ID: 00457-40173 V1.50-130218.
54. Finnigan, M. *5 Great B-3 Drawbar Settings*; Keyboard Magazine: San Bruno, CA, USA, 2012.
55. Xavier Serra. "El Cant dels Ocells." 27 January, 2013. Used under Creative Commons Attribution 3.0 Unported (https://creativecommons.org/licenses/by/3.0/), Available online: https://www.freesound.org/people/xserra/sounds/176098/ (accessed on 21 March 2016).